Future Technology
Open Access Journal
ISSN 2832-0379

November 2026| Volume 05 | Issue 04 | Pages 01-14

Journal homepage: https://fupubco.com/futech

https://doi.org/10.55670/fpll.futech.5.4.1

Future Publishing LLC

Article

A framework for integrating artificial neural networks and finite element analysis for shear strength prediction in unreinforced RC beam–column joints

Ranim Maatouq, Rouya Hdeib*

Department of Civil and Architectural Engineering, Applied Science University, Al-Ekir, Bahrain

ARTICLE INFO

Article history:
Received 27 January 2026
Received in revised form
05 June 2026
Accepted 10 July 2026

Keywords:
Artificial neural network (ANN),
Finite element analysis (FEA),
Reinforced concrete, Beam-column joint,
Shear strength prediction, Seismic resilience

*Corresponding author
Email address:
Rouya.hdeib@asu.edu.bh

DOI: 10.55670/fpll.futech.5.4.1

ABSTRACT

Beam-Column joints (BCJs) are critical components in reinforced concrete (RC) buildings. These members experience excessive stress during seismic events, often resulting in catastrophic failures, particularly in RC buildings constructed prior to the introduction of seismic design provisions and lacking reinforcement in the BCJ zone. The study presents a machine learning framework to predict the shear strength of unreinforced BCJs using 7 input parameters. This study developed an Artificial Neural Network-Finite Element Analysis hybrid model (ANN-FEA-13), trained, validated, and tested on 4320 samples of BCJ failure generated through nonlinear analysis in ABAQUS. The data was divided into training (70%), testing (15%), and validation (15%) sets. The ANN-FEA-13 model achieved high prediction accuracy (R = 0.962) and was compared with experimental data from literature and the ACI 318 code, showing superior performance. The results were promising and demonstrated the effectiveness of the developed data-driven ANN-FEA-13 framework, which reliably predicts BCJ failure and supports ongoing efforts in resilience-based assessment and retrofitting of aging RC structures in seismic regions.

1. Introduction

Reinforced concrete (RC) structures form the backbone of modern infrastructure worldwide. Many existing RC buildings were constructed before the development of seismic design provisions in the code [1], making them vulnerable to lateral loads, such as earthquakes, due to inadequate or absent transverse reinforcement at beam-column joints (BCJs) [2]. The BCJ is a critical region that maintains global structural stability and continuity. Shear failure localized in this region can trigger partial or complete collapse [3]. Such vulnerabilities remain widespread in aging buildings across Asia, Latin America, and the Middle East [4]. This challenge is directly tied to urban resilience, as the failure of non-ductile joints undermines community safety and post-event functionality [5,6]. Earlier experimental studies strongly recommended including both transverse and vertical joint reinforcement to ensure adequate shear capacity. However, unreinforced BCJs in older buildings still exhibit inadequate shear strength under seismic loads, highlighting the need for reliable assessment and retrofitting strategies aligned with resilience-based design frameworks [7]. Several studies investigated the behavior and retrofitting of reinforced BCJs using Fiber-reinforced polymers (FRP), steel jacketing, or other hybrid materials [8-12]. Yet only a few studies have focused on predicting the strength of unreinforced BCJs, a critical gap in understanding the seismic vulnerability of pre-code RC frames [13]. Developing such predictive tools is vital for ensuring structural safety and supporting resilience-oriented retrofitting decisions [14]. Machine learning (ML), a subset of artificial intelligence (AI), enables computational systems to learn patterns from data without explicit programming [15]. Among various ML approaches, artificial neural networks (ANNs) are particularly effective in modeling nonlinear relationships between input and output variables, offering strong predictive accuracy in regression-based problems [16,17]. ML methods have increasingly been used in civil engineering to solve complex, time-sensitive, and cost-dependent problems. Among various ML techniques, ANN has shown promising accuracy [18,19]. Example applications include seismic design

of bridge piers [20], concrete strength prediction [21], seismic performance of corroded reinforced concrete buildings [22], crack detection [23], and labor productivity [16]. Recent studies further demonstrated that hybrid ML systems can enhance resilience analysis and decision-making [24-26]. Multiple ML frameworks have been developed for predicting the shear strength of reinforced RC-BCJs. For example, Mangalathu & Jeon (2018) [17] classified BCJ failure modes using ML, Alwanas et al. (2019) [27] proposed an extreme learning machine (ELM) model, and Marie et al. (2022) [28] compared different ML techniques under cyclic loading. Haido (2022) [2] and Ramavath & Suryawanshi (2024) [29] validated ANN-based models for reinforced joints with high accuracy. However, no comprehensive ML model exists for unreinforced BCJ, which remain common in older structures and represent a key weakness in the resilience of RC frames [7,26].

The size and quality of training data are crucial factors that significantly influence the accuracy and performance of ML models [15]. Existing studies typically rely on limited experimental data, which constrains model robustness and particularly undermines the effectiveness of ANN techniques, which thrive on substantial datasets for optimal learning. Advances in nonlinear finite element analysis (FEA) software, in conjunction with improved computational efficiency, enable the generation of large amounts of required data for training and validating predictive models [30,31]. These advances offer a unique opportunity to model and generate a large dataset that replicates experimental results and supports training and validation of predictive models. This approach aligns with the hybrid modeling paradigm adopted in recent structural resilience publications, where simulation and ML are integrated to predict complex structural behavior [25,32]. Integrating simulation-driven datasets with AI-based learning thus represents a scalable pathway to model complex joint behavior beyond the limits of physical testing.

Despite notable progress in ML and FEA applications, the shear behavior of unreinforced BCJs remains unmodeled. Therefore, this study proposes "ANN-FEA-13", a hybrid predictive framework that combines FEA-simulated data and ANN modeling to estimate the shear capacity of unreinforced exterior RC BCJs subjected to monotonic loading. Using 4,320 data samples generated through ABAQUS simulations [33], the model is compared with published experimental studies and demonstrates strong potential as a resilience-oriented assessment tool. The framework contributes to performance-based retrofitting strategies by linking predictive accuracy with decision-making resilience metrics such as those proposed by Mucedero et al. (2025) [14].

2. Materials and methods

2.1 Beam-column joint modeling

Six primary design parameters and one derived parameter influencing BCJ shear strength were varied to generate the dataset (Table 1). These include column depth (h_c), beam depth (h_b), concrete cylinder compressive strength ($f'c$), beam tension steel area (A_{st}), beam tension reinforcement yield strength (f_y), and axial column load as a ratio of its capacity (P_y). The seventh parameter is the joint area Aj (b_j x h_c) derived based on variable column depth h_c and constant beam width b_j. These parameters were selected based on their established impact on joint shear behavior reported in the literature [12,13]. A total of 6480 configurations were simulated using ABAQUS/CAE 6.13-1 version nonlinear analysis, out of which 4320 samples showing joint shear failure were selected for ANN modeling (Figure 1).

Table 1. Discrete levels of input parameters selected for the FEA simulation. The total **design size is 6480 joint configurations, out of which 4320 cases of joint shear failure were filtered for ANN training/validation and testing

Parameter	Symbol	Unit	levels (n)	Discrete values
Concrete cylinder compressive strength	f'_c	MPa	10	17, 20, 25, 30, 35, 40, 45, 50, 55, 60
Column depth	h_c	mm	6	150, 200, 300, 400, 500, 600
Beam depth	h_b	mm	6	150, 200, 300, 400, 500, 600
*Column axial-load ratio	P_y	-	3	0.05, 0.10, 0.15
Tension steel area (beam)	A_{st}	mm^2	3	3Ø16 (603), 3Ø20 (942), 3Ø25 (1473)
Steel yield strength (beam)	f_y	MPa	2	460, 660
Joint area	A_j	mm^2	6	Derived parameter based on variable column depth and fixed beam width ($A_j = b_j$ x h_c)

* The Axial load ratio $P_y = N/(b_j \times h_c \times f'_c)$ is dimensionless. Where N is the column axial load (N), b_j is the joint width (mm), and f'_c is the concrete compressive strength of the column (MPa).
**The Design size: $10 \times 6 \times 6 \times 3 \times 3 \times 2 = 6480$ joint configurations, out of which 4320 cases were filtered for joint shear failure and used for ANN training/validation.

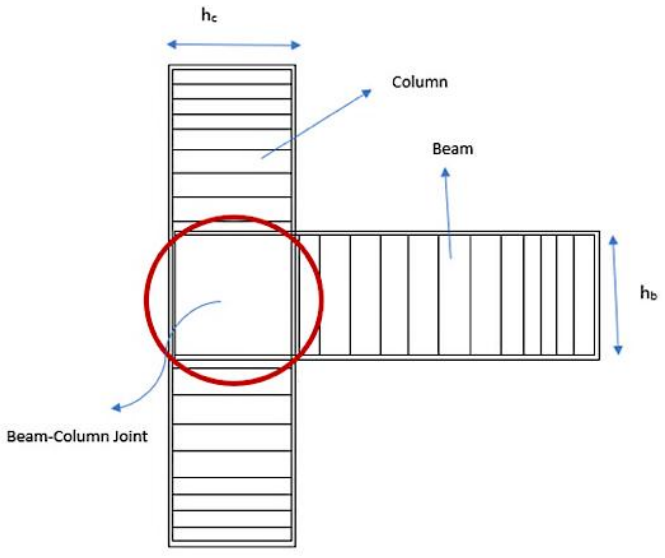

Figure 1. The unreinforced exterior BCJ configuration used in the simulations

In Figure 2, a correlation matrix is presented for the inputs and output parameters. It illustrates that concrete compressive strength has the highest contribution to the BCJ shear strength, with a positive correlation, while the column depth has the second-highest contribution but is negatively correlated with the joint shear strength. The dependent parameter (joint area) is correlated with the column depth. A key advantage of the machine learning -ANN technique is its lower sensitivity to multicollinearity compared to other traditional regression models [34]. ANNs do not require independence assumptions; their hidden layers can learn non-linear interactions between inputs despite the dependence of their linear relations. Moreover, a preprocessing technique is applied to the data. In this research, a joint area-dependent input parameter was added to improve accuracy, yielding a small improvement in the model's accuracy during trial-and-error training of the ANN.

Figure 2. A correlation matrix is presented for the inputs and output parameters

2.2 Finite element analysis (FEA) framework

Nonlinear 3D finite element analyses were conducted using ABAQUS 6.13-1 (2013) [33] to simulate the structural response of unreinforced exterior BCJs. Concrete was modeled with the Concrete Damage Plasticity (CDP) model, which accounts for compressive crushing and tensile cracking. The CDP model parameters were defined following previous research [3,8] and are summarized in Table 2. The dilation angle of concrete, taken as 36°, is the angle that causes plastic shearing due to volumetric strain. A study by Ajmal et al. [35] recommended that the dilatation angle be between 30 and 36 degrees for BCJs that fail in shear. Similarly, in reinforced concrete seismic design, the ABAQUS user manual [33] recommends taking the dilation angle between 35 and 38°. In addition, eccentricity is another plasticity parameter that represents the deviation from the center; its default value is 0.1. Moreover, the ratio of biaxial loading (f_{b0}) to uniaxial loading (f_{c0}) is a plasticity parameter, and it is typically taken as 1 or larger. In this research, the value 1.16 was used, as it is the default value. Furthermore, the ratio between the second stress invariant on the tensile meridian to that on the compressive meridian (K) was taken as 0.667, which is the default value. The concrete modulus of elasticity (E_c) is calculated as Ec = 4700 $\sqrt{f'_{c0}}$ MPa according to the ACI code [36], and the concrete Poisson's ratio = 0.19, while the density of concrete is taken as 24 kN/m³.

Table 2. The concrete damage plasticity (CDP) model parameters for concrete

Property	Symbol	Value / Relation	Reference
Density	ρ	24 kN/m³	–
Elastic modulus	E_c	4700 $\sqrt{f'_{c0}}$ (MPa)	[36]
Poisson's ratio	ν	0.19	–
Dilation angle	ψ	36°	[35]
Eccentricity	ε	0.1	[33]
f_{b0}/f_{c0}	–	1.16	Default
K (tensile/compressive meridian ratio)	–	0.667	Default

The uniaxial stress–strain relation for unconfined concrete in compression follows Mander et al. [37]. Previous studies used the Mander model to predict concrete behavior in compression, and the results demonstrated its ability to accurately capture compressive behavior [38-40].

$$f_c = \frac{f'_{c0} \times \frac{\varepsilon_c}{\varepsilon_{c0}} \times r}{r - 1 + \left(\frac{\varepsilon_c}{\varepsilon_{c0}}\right)^r} \quad (1)$$

$$r = \frac{E_c}{E_c - E_{sec}} \quad (2)$$

$$E_{sec} = \frac{f'_{c0}}{\varepsilon_{c0}} \quad (3)$$

$$\varepsilon_c^{in} = \varepsilon_c - \varepsilon_{oc}^{el} \quad (4)$$

$$\varepsilon_{oc}^{el} = \frac{0.3 \times f'_c}{E_c} \quad (5)$$

Where f_c is the concrete compressive stress, f'_{c0} is the unconfined ultimate concrete cylinder compressive strength, ε_c is longitudinal compressive concrete strain, ε_{c0} is the unconfined concrete strain at the ultimate compressive strength, and E_c is the tangent modulus of elasticity of concrete. The inelastic strain (ε_c^{in}) is calculated by deducting the elastic strain (ε_{oc}^{el}) from the total strain (ε_c). The elastic strain of concrete is taken as (0.3×f'c/Ec), since it is recommended to limit the elastic strain to 30% of the concrete compressive strength. The CDP inputs entered by the user for the concrete material property, with different strengths generated using the Mander model for concrete compressive strength. For concrete tension behavior, a linear-elastic, brittle material with strain softening was used, and tension stiffening was achieved by modifying the softening behavior of the concrete. Tensile behavior was modeled using the modified Massicotte et al. [41] model with tension stiffening. Post-cracking tensile stress-strain curves for different concrete strengths were generated using the modified Massicotte et al. [41] model and then entered into ABAQUS. Damage parameters in compression (d_c) and tension (d_t) were determined using the ABAQUS formulation:

$$d_c = 1 - \frac{f_c \times E_c^{-1}}{\varepsilon_c^{in}\left(\frac{1}{b_c} - 1\right) + f_c \times E_c^{-1}} \quad (6)$$

$$d_t = 1 - \frac{f_t \times E_c^{-1}}{\varepsilon_t^{in}\left(\frac{1}{b_t} - 1\right) + f_t \times E_c^{-1}} \quad (7)$$

Steel reinforcement bars were modeled (Figure 3) using 2-node linear truss elements (T3D2) with an elastic–plastic bilinear stress–strain relation (Es = 200 GPa, ν = 0.3). Yield strengths of 460 MPa and 660 MPa were assigned depending on the specimen configuration. Concrete and steel plates were meshed using reduced integration 8-node brick elements (C3D8R). The simulations were performed by varying the mesh sizes (20 mm, 30 mm, and 40 mm) to assess the effect of mesh size on the accuracy of the analysis, as shown in Table 3. Although the 20 mm mesh size slightly improved the agreement with the experimental ultimate load, the improvement was limited compared to the 30 mm mesh size. Furthermore, the 20 mm mesh-size simulation required significantly more computational time than the 30 mm mesh-size simulation (2-3 times longer). The 40 mm mesh size required less computational time but led to a large deviation, reducing the predicted ultimate load by approximately 10.5%. Therefore, the 30 mm mesh was adopted for the simulation as a suitable compromise between computational time and prediction accuracy. Boundary conditions were defined as follows:

- Column top restrained in x–z; bottom fixed in x–y–z.
- Axial column load applied as uniform pressure on the top surface.
- Beam tip loaded via controlled vertical displacement (36 mm) through a reference node tied to the loading plate.

The reinforcement model was developed using one-dimensional rods (rebar), as shown in Figure 3. The mesh model for the FEA numerical simulation is shown in Figure 4. The applied loads and boundary conditions are shown in Figure 5.

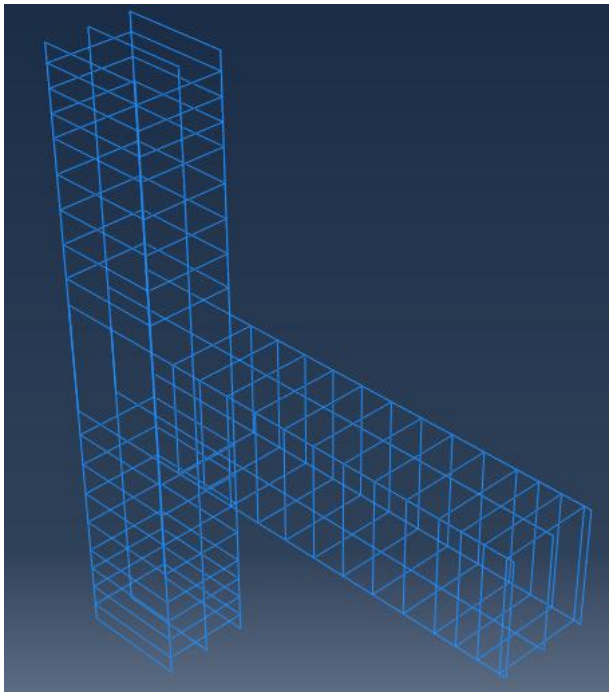

Figure 3. Reinforcement modeling in ABAQUS

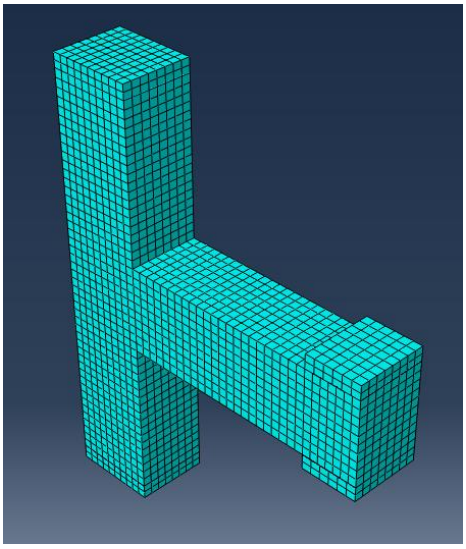

Figure 4. The meshing of the numerical simulation for a BCJ model

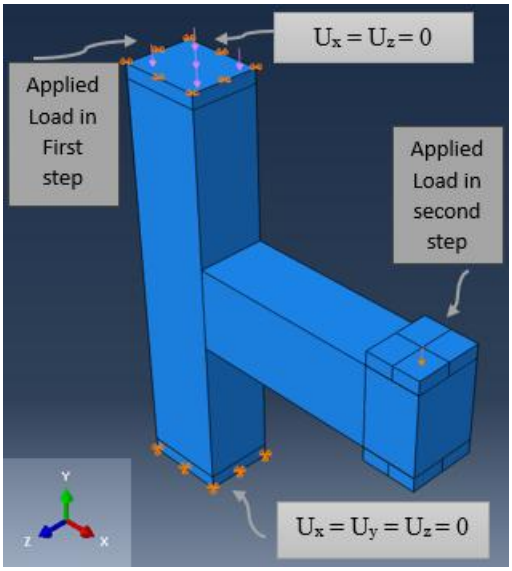

Figure 5. Applied loads and boundary conditions for the BCJ model

Table 3. Mesh refinement effects on ultimate load and computational cost

Mesh Size	Peak load (KN)	Analysis time	Deviation with the experimental load
Experimental Result	122.46	-	-
20 mm	125.4	Very long	2.08 %
30 mm	127.3	Relatively long	3.95 %
40 mm	135.29	Relatively short	10.48%

2.3 Validation with experimental data

The FEA results were validated against an experimental test conducted by Ajmal (2016) [42] on an exterior BCJ. The specimen had f'c = 45 MPa, fy = 607 MPa, and dimensions of 250 × 300 mm for both beam and column. The base model included six Ø20 longitudinal column bars, three Ø20 top and bottom beam bars, and Ø8 @ 50 mm stirrups, as summarized in Table 4. The stirrups existed outside the joint core, whereas the joint region itself was clear and had no transverse reinforcement. To verify the accuracy of the Concrete Damage Plasticity (CDP) formulation, the simulated stress–inelastic strain curve for concrete in compression was compared with the experimentally derived curve from the reference specimen (Figure 6). The two curves show close agreement, confirming that the adopted CDP parameters and the Mander model accurately captured the nonlinear compressive response and post-peak softening behavior of the concrete. The global load–displacement response of the model also correlated well with the experimental results. The experimental ultimate load (122.46 kN at 20.46 mm displacement) compared closely with the FEA-predicted value (127.3 kN at 18 mm), yielding a 3.95% deviation, confirming the accuracy of the simulation (Figure 7). This consistency across both the material-level and structural-level responses validates the robustness of the proposed numerical setup. Stress distributions and damage propagation at the ultimate load are illustrated in Figures 8–10, which show consistent failure localization at the joint core. The validated model was therefore adopted to generate the full 4320-sample dataset for ANN training and testing.

Table 4. Experimental base model characteristics [39]

Parameter	Value	Unit
f'c	45	MPa
f_y	607	MPa
Column longitudinal reinforcement	6Ø20	–
Beam longitudinal reinforcement	3Ø20	–
Stirrups	Ø8 @ 50 mm	–

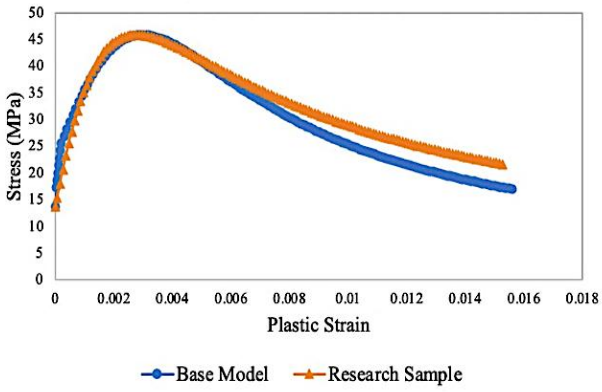

Figure 6. Comparison between experimental and simulated concrete stress–inelastic strain curves, demonstrating strong agreement and validating the CDP material model

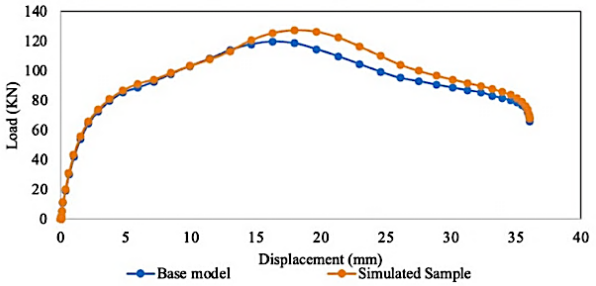

Figure 7. Comparison of experimental and FEA load–displacement curves of the base BCJ specimen

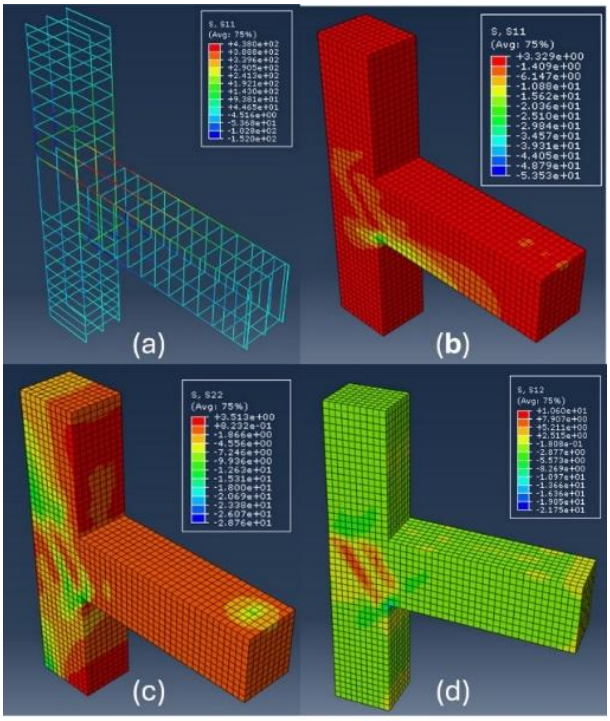

Figure 8. Stress and damage contours at ultimate load for validated BCJ model. (a) Steel stresses (b) Stress S11 in concrete (c) Stress S22 in concrete (d) Stress S12 in concrete

Among all simulated samples, only shear-failure samples were selected and retained for ANN modeling. We distinguish between three main types of BCJ failure: shear failure at the joint, flexural failure, and anchorage failure [43]. This study focused on developing a shear-strength prediction model; therefore, only samples that failed in shear were included. The contours for each sample were checked to recognize the concrete damage at the joint region, as shown in Figure 9 and Figure 10. Moreover, the stress at failure for tensile rebar (S11) was recorded across the entire dataset to exclude samples that failed in flexure. The yield stress used for the rebar in ABAQUS was set to the yield stress at failure (460 MPa or 660 MPa). If S11 at failure exceeded this value, the sample was eliminated. Figure 8(d) shows the in-plane stress S12, indicating joint failure in shear.

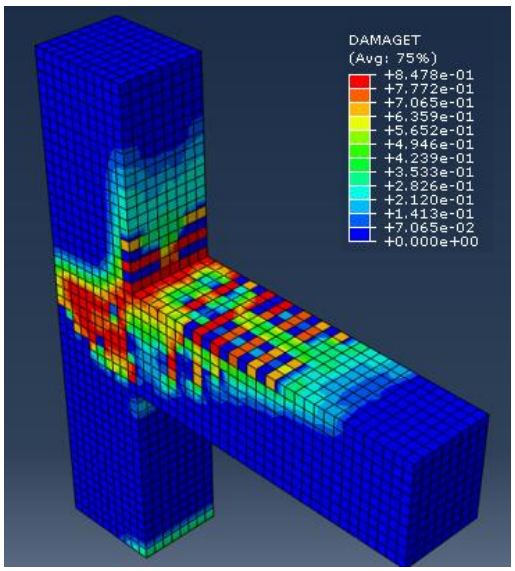

Figure 9. Concrete Tension damage at the ultimate load corresponding to 18 mm displacement for the simulated sample

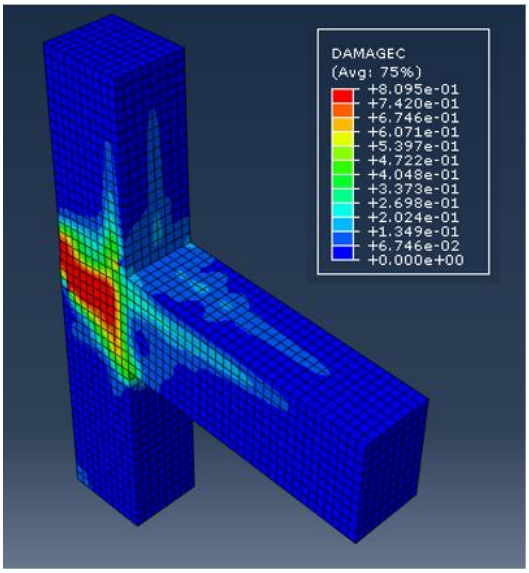

Figure 10. Concrete Compression damage at the ultimate load

2.4 Artificial neural network (ANN) modeling

Data preparation and normalization: An ANN was used to develop a prediction model for the shear strength of unreinforced BCJ using the feedforward backpropagation network (FFBPN) [23], with MATLAB software [44] and the neural network tool (nftool). The dataset used for ANN training was derived from 4320 validated FEA simulations representing the shear failure of unreinforced RC beam–column joints (BCJs). Each record included seven independent variables and one dependent output, the joint shear strength (V_j). Before training, the data were normalized using min–max scaling within the range [–1, 1] using Eq (8), which enhances model convergence and prevents variables with large magnitudes (e.g., A_{st}, A_j) from dominating the learning process [45].

$$a_n = 2 \times \left(\frac{a_i - a_{min}}{a_{max} - a_{min}}\right) - 1 \quad (8)$$

where a_i is the raw variable, and a_{min}, a_{max} are its minimum and maximum training-set values, which will remain constant in the future use of the ANN model. Normalization was performed using MATLAB's built-in pre-processing utilities (nftool). The dataset was randomly divided using MATLAB function into 70% training, 15% testing, and 15% validation subsets to prevent over-fitting and to ensure that generalization could be objectively assessed [46].

Network architecture and training: A multi-layer feed-forward neural network (ML-FFNN) was adopted due to its proven ability to generalize to complex, nonlinear regression problems in structural engineering [18,21]. The architecture of the ML-FFNN consists of one input layer, one or more hidden layers, and one output layer. The complexity of the problem will define the number of hidden layers and the number of neurons in each hidden layer. The model architecture consisted of the following three layers:

- Input layer: seven neurons corresponding to the design variables (hc, h_b, f'c, Ast, fy, Py, Aj).
- Hidden layer: one hidden layer with an optimized number of neurons determined through trial convergence using RMSE minimization.
- Output layer: one neuron producing the predicted joint shear strength (Vj).

The neuron-level transformation is expressed as shown in Eq (9):

$$a = f(W \times P + B) \quad (9)$$

where a is the neuron output vector, W is the connection-weight matrix, P the input vector, B the bias, and f the activation function.

The hyperbolic tangent sigmoid function Tansig(x) was selected for the hidden layer, which is a nonlinear transfer function allowing to capture the nonlinearity in the relationship between input and output parameters, and performs efficiently on normalized data in [–1, 1]. A linear (Purelin(x)) activation was selected for the output layer which is suitable for continuous regression outputs and avoids saturation effects. Alternative activations (e.g., Logsig) were evaluated but offered no performance gain while increasing computational costs. The Levenberg–Marquardt (trainlm) back-propagation algorithm was employed for weight optimization, as it combines the rapid convergence of the Gauss–Newton method with the stability of gradient descent, making it particularly effective for medium-sized networks (≤ 5000 samples) [44]. This method has consistently outperformed other algorithms, such as scaled conjugate gradient (SCG) and resilient backpropagation (Rprop), in structural prediction studies [17,47].

The training process was repeated consistently while tuning the ANN model's hyperparameters to optimize performance. The gradient during the training process measures the steepness of the error surface; values approaching zero indicate better model convergence. Figure 11 shows that the gradient reached 0.0017336 at epoch 65, indicating good convergence of the model. Furthermore, the parameter (μ) controls the step size in the Levenberg–Marquardt training algorithm, where it is very near to zero, indicating stable training and convergence. In addition, the validation check stopped at 6 to avoid overfitting. A trial-and-error evaluation of different hidden-neuron configurations (10–20 neurons) was used to select the ANN model architecture. The final ANN-FEA-13 model architecture, formed of 1 hidden layer and 13 neurons, was found to provide the lowest prediction error and the highest

correlation among the tested model configurations. Furthermore, the Neural Network Toolbox in MATLAB can automatically monitor model performance and validation during training, supporting the evaluation process and reducing the likelihood of overfitting. The number of nodes in the hidden layer was selected before each training trial and optimized to achieve higher accuracy. Figure 12 presents the optimization of the number of nodes in the hidden layer, used to compare the MSE of the validation set with its variation. Figure 13 shows the predicted and actual shear strength in the testing set. An ANN model generalizes well to future data when the error is small [48].

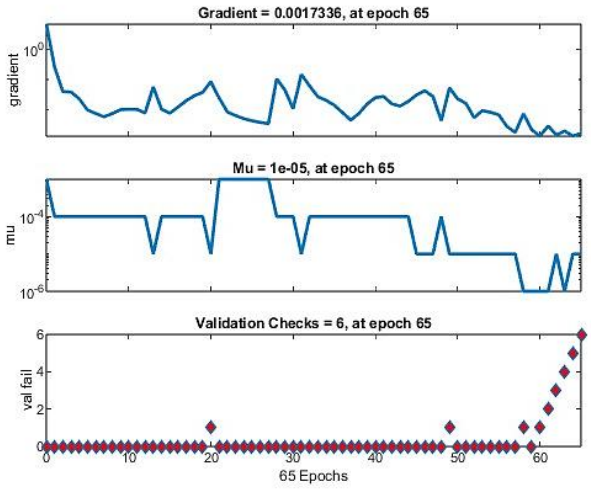

Figure 11. ANN training state showing gradient, μ parameter, and validation checks during the training process

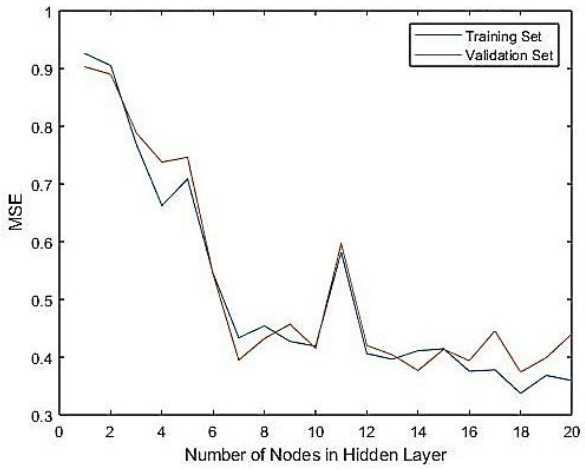

Figure 12. Optimizing the number of nodes in the hidden layer

Model performance evaluation and optimization: The ANN network performance was assessed using four performance measures, as shown in Eqs. (10), (11), (12), and (13):

$$RMSE = \sqrt{\frac{\sum_{i=1}^{n}(A_i - Y_i)^2}{n}} \quad (10)$$

$$MSE = \frac{1}{n}\sum_{i=1}^{n}(A_i - Y_i)^2 \quad (11)$$

$$R = \frac{\sum_{i=1}^{n}(A_i - \hat{A})(Y_i - \hat{Y})}{\sqrt{\sum_{i=1}^{n}(A_i - \hat{A})^2 \sum_{i=1}^{n}(Y_i - \hat{Y})^2}} \quad (12)$$

$$R^2 = \frac{\sum_{i=1}^{n}(A_i - \hat{A})^2 - (Y_i - \hat{Y})^2}{\sum_{i=1}^{n}(A_i - \hat{A})^2} \quad (13)$$

where A_i and Y_i are the expected and predicted output values, respectively. $\hat{A}$ and $\hat{Y}$ are the average expected and predicted output values, respectively. n is the number of data points.
The mean squared error (MSE) is used for performance analysis during training to assess the error between the network's predicted and expected outputs. The root mean square error (RMSE) quantifies the magnitude of prediction error and is used to optimize the number of neurons in the hidden layer, as smaller RMSE values consistently indicate improved generalization across the testing and validation subsets. The coefficient of correlation (R) measures the accuracy of an ANN model, where R = 1 indicates a perfect correlation between predicted and expected values. The coefficient of determination (R^2) evaluates how well a model fits the data and quantifies its predictive accuracy. The combination of these evaluation indices allows robust evaluation of both precision (error magnitude) and trend fidelity (correlation). The error histogram for the proposed ANN model is shown in Figure 14, covering the full data sets of 4320 connection samples.

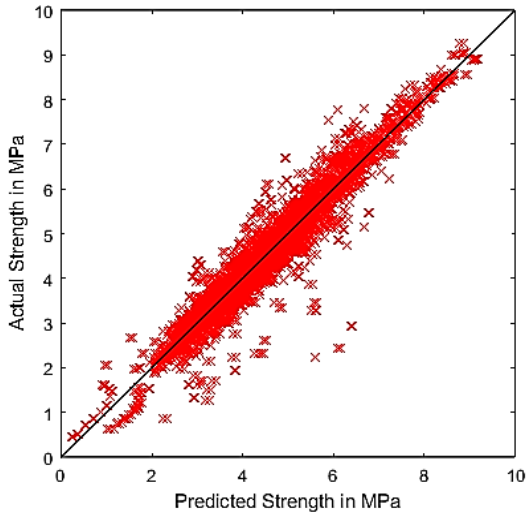

Figure 13. Predicted Vs. Actual shear Strength of the unreinforced joint

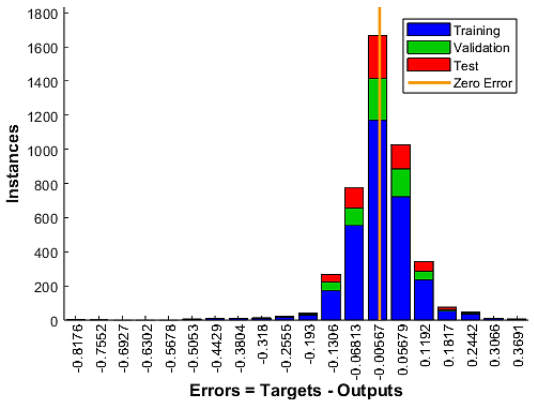

Figure 14. Error Histogram of the data sets in (MPa)

Figure 15 presents the flow diagram of the proposed integrated framework for developing the ANN-FEA-13 model for shear strength prediction of unreinforced BCJs. Table 5 and Table 6 summarize the input/output parameters and descriptive statistics of the dataset used for model development. The wide variation in values across variables ensured sufficient diversity, allowing the ANN model to effectively learn the nonlinear interactions among geometry, material properties, and shear response.

Table 5. Input and output variables used for ANN–FEA-13 development

Variable	Symbol	Description	Unit
Input Variables			
X_1	h_c	Column depth	mm
X_2	h_b	Beam depth	mm
X_3	$f_{c'}$	Concrete compressive strength	MPa
X_4	A_{st}	Total area of beam tension reinforcement	mm^2
X_5	f_y	Yield strength of beam tension reinforcement	MPa
X_6	P_y	Column axial-load ratio ($\approx N / b_j \times h_c \times f'c$)	-
X_7	A_j	Effective joint area ($b_j \times h_c$)	mm^2
Output Variable			
Y	V_j	Shear strength of joint region (target)	MPa

3. Results and discussion

3.1 The ANN-FEA-13 model architecture and performance

The optimal network configuration for the proposed Artificial Neural Network-Finite Element Analysis hybrid model ANN-FEA-13 Model comprised seven input neurons corresponding to the selected design parameters, one hidden layer with thirteen neurons representing parameters created from the network itself, and one output neuron representing the joint shear strength. This architecture was selected after iterative trials that minimized the mean-squared error (MSE) while maintaining a high correlation coefficient (R). The final ANN-FEA-13 model architecture is illustrated in Figure 16 showing the connections of weights and bias, while Table 7 summarizes the statistical performance across training, validation, and testing datasets.

The model achieved R values of 0.961, 0.967, and 0.956 for training, validation, and testing datasets, respectively, yielding an overall correlation of 0.962 (Figure 17). The corresponding RMSE values were consistently below 0.37 MPa, confirming the Model's stable generalization and robustness. These results demonstrate that the ANN–FEA-13 model can effectively capture the nonlinear interactions among design parameters influencing joint shear strength, providing a reliable alternative to conventional analytical equations.

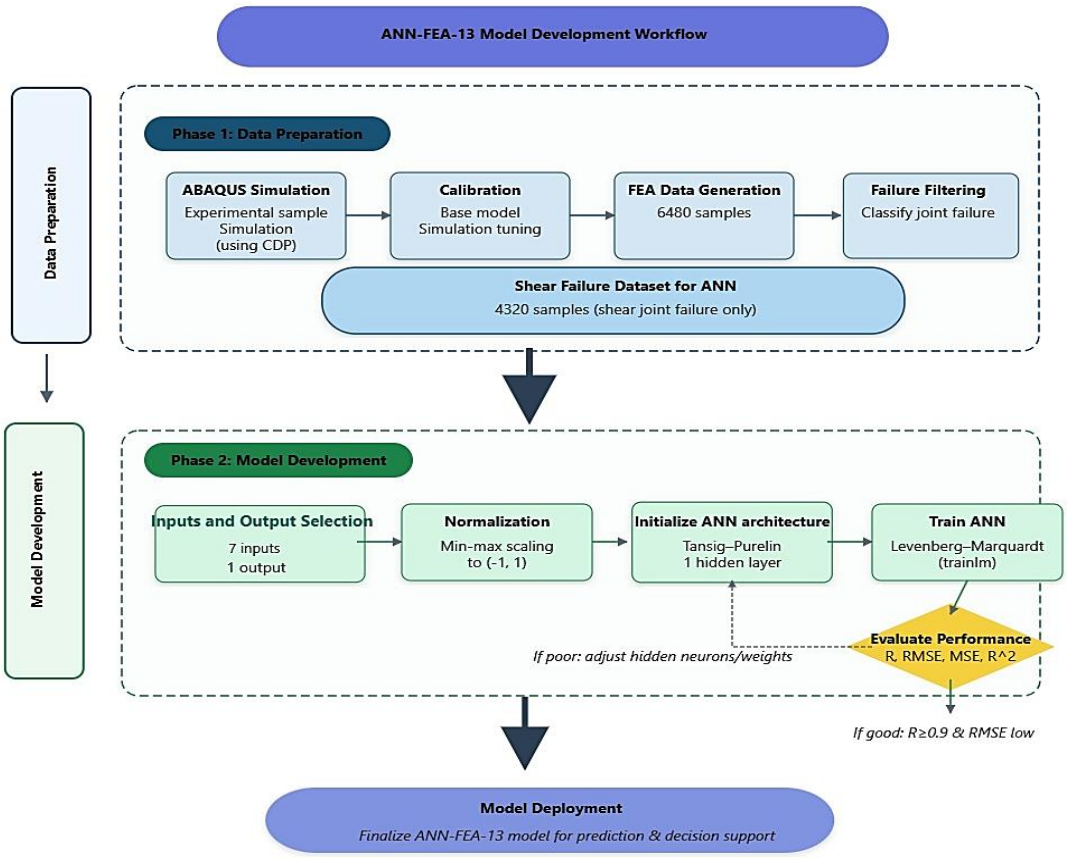

Figure 15. The flowchart of the integrated framework for the ANN–FEA-13 model development for predicting shear strength of unreinforced BCJs. Phase 1 outlines the integrated process for BCJ model development, FEA data generation, and joint failure classification. Phase 2 outlines the process for data normalization, ANN architecture setup, iterative training, and performance evaluation and optimization.

Table 6. Statistical characteristics of the input and output variables

Variable	Symbol	Units	Minimum	Maximum	Mean	Standard Deviation
Column Depth	h_c	mm	150	600	301.4	146.8
Beam Depth	h_b	mm	150	600	353.0	159.1
Concrete Compressive Strength	$f'c$	MPa	17	60	35.2	13.9
Beam Reinforcement Area	A_{st}	mm²	603	1473	1118.7	348.6
Beam Yield Strength	f_y	MPa	460	660	577.6	98.4
Axial Column load as ratio	P_y	-	0.05	0.15	0.099	0.041
Joint Area	A_j	mm²	37 500	150 000	75 356	36 699
Shear strength of BCJ	V_j	MPa	0.46	9.25	4.52	1.43

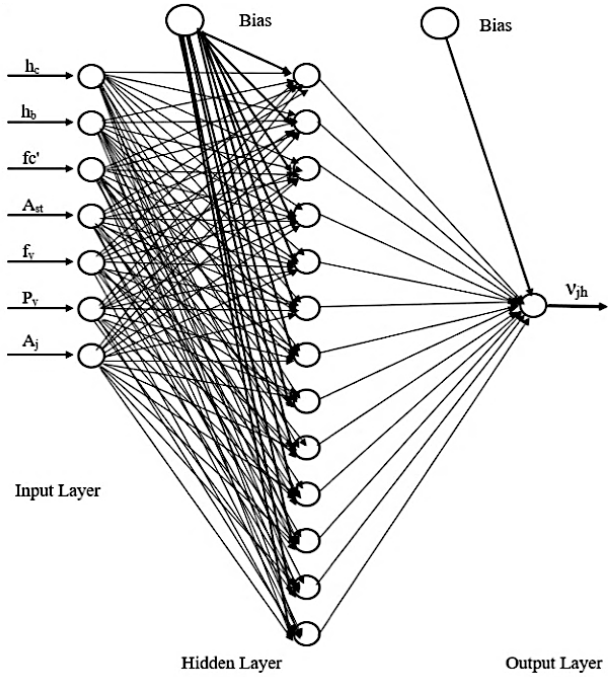

Figure 16. Structure of the ANN-FEA-13 model showing weights and bias connections

3.2 Mathematical representation of the model

The ANN-FEA-13 model is formulated as a set of mathematical equations that describe the supervised nonlinear mapping from 7 input parameters to the predicted shear strength of the exterior RC beam-column joint. To facilitate reproducibility, the developed ANN–FEA-13 model structure was represented mathematically as weighted sums and activation functions. The hidden neuron behavior is governed by Equation (13), and the overall activation/transfer formulation follows the general multilayer feed-forward network structure, expressed as:

$$K_i = \sum_{j=1}^{7} [W_{ij} X_j] + b_i \quad (14)$$

$$Y_{output} = f_{out}(\sum_{i=1}^{13} [W_i' f_h(K_i)] + b_o) \quad (15)$$

where

- X_j is the normalized input parameters $(h_c, h_b, f_c', A_{st}, f_y, P_y, A_j)$
- W_{ij} and b_i are the weights and biases for each hidden neuron K_i.
- f_h is the hyperbolic tangent sigmoid activation function,
- W_i' and b_o are the output-layer weights and bias, and
- f_{out} is the linear transfer function (purelin) used for the output neuron.

The hyperbolic tangent sigmoid transfer function $f_h(K_i)$ is expressed as:

$$f_h(K_i) = \frac{2}{1+e^{-2K_i}} - 1 \quad (15)$$

which allows the network to capture the complex nonlinear relationships between structural parameters and joint shear capacity. The output neuron employs a linear transfer function (purelin) as shown in Eq. (16). Reverse normalization relationship derived during preprocessing (Eq. 17) restores the final ANN predicted output value to its real-scale shear strength in MPa. This conversion restores the original physical units and facilitates direct comparison with FEA and experimental results:

$$\text{purelin}(Y_{output}) = Y_{output} = \sum_{i=1}^{13} [W_i' f_h(K_i)] + b_o \quad (16)$$

Table 7. Performance evaluation of the ANN-FEA-13 model for training, validation, and testing datasets

Model		ANN-FEA-13
Training Dataset (3024 Samples)	*RMSE*	0.347
	MSE	0.1207
	R	0.961
	R²	0.924
Validation Dataset (648 Samples)	*RMSE*	0.351
	MSE	0.141
	R	0.967
	R²	0.935
Testing Dataset (648 Samples)	*RMSE*	0.367
	MSE	0.172
	R	0.956
	R²	0.914

The corresponding input and output parameters used for ANN-FEA-13 are summarized earlier in Table 4. The weights and biases of the output layer are presented in Table 8. The complete set of the neuron weights and biases for the hidden layer is presented in Table 9. To maintain conciseness, only the key equations, resultant weights, and biases are presented herein; the complete neuron-weight relationships and equations, in addition to the developed MATLAB code for the

ANN-FEA-13 model, are provided in Appendix A for reproducibility. This representation facilitates the engineering use of the model to predict shear strength in unreinforced exterior joints.

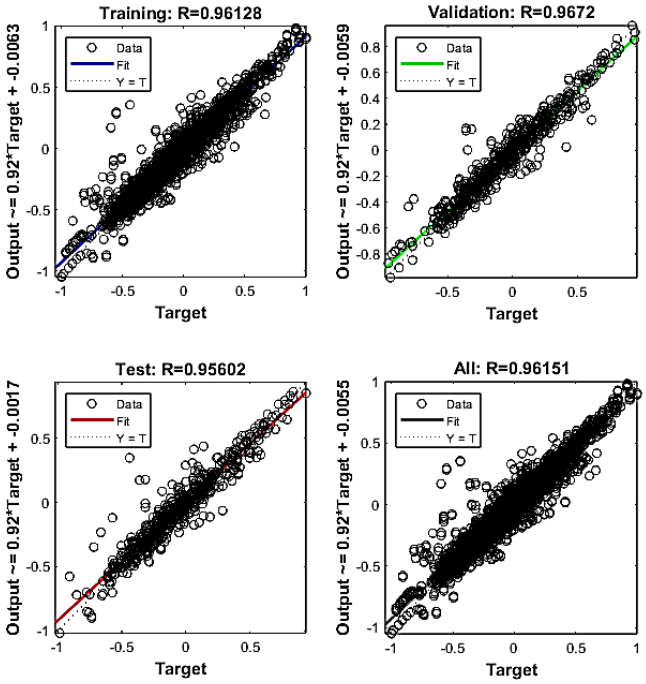

Figure 17. Regression plots showing the correlation (R) for training, validation, and testing phases

3.3 Comparison with ACI-318 Code Predictions

The predictive accuracy of the ANN-FEA-13 model was benchmarked against the ACI-318 provisions for shear strength of the joint region using the full testing dataset (648 exterior connections). Figure 18 shows the results for selected 100 samples from the testing data set comparing ACI 318, ANN-FEA-13, and the baseline FEA prediction.

Table 8. The resultant weights and bias for the output layer of the developed ANN-FEA-13 model for the prediction of shear strength of unreinforced BCJs. The full set of equations is provided in Appendix A3 for reproducibility

Output Weight	Value
W'_1	+0.5997
W'_2	+0.6566
W'_3	-0.1274
W'_4	-0.6396
W'_5	+1.1219
W'_6	+1.9717
W'_7	+1.9659
W'_8	+0.0292
W'_9	+0.2192
W'_{10}	-2.3402
W'_{11}	-1.3293
W'_{12}	+0.5239
W'_{13}	-2.4671
Bias b_o	-0.2427

Table 9. The resultant weights and biases for the hidden layer of the developed ANN-FEA-13 model for the prediction of shear strength of unreinforced BCJs. The full set of equations is provided in Appendix A2 for reproducibility

Neuron	W_{hc}	W_{hb}	W_{fc}	W_{Ast}	W_{fy}	W_{Py}	W_{Aj}	Bias b
K_1	-0.5185	-1.2716	-0.6639	-2.4119	-0.0160	-0.0172	-0.5546	+1.3476
K_2	-0.3564	-0.2010	+0.1107	+0.3687	+0.0181	+0.1010	+0.0468	-0.1554
K_3	+1.0215	+1.5968	+1.8751	+0.1720	-0.0711	+0.1343	+1.3570	-0.9316
K_4	-1.1757	-1.2049	-0.6131	-1.9716	-0.0044	+0.0106	+0.2407	+1.1729
K_5	-1.6588	+1.9250	-0.2070	+0.3456	+0.0453	-0.0128	-3.1511	-3.8005
K_6	-0.1273	+3.2528	-0.1104	-0.1829	-0.0090	-0.1661	+1.4606	+4.7283
K_7	-0.7594	-6.5145	+0.1309	+0.1816	+0.0031	+0.1362	-0.5558	-7.8068
K_8	+1.1948	+1.4796	-0.5909	-1.1049	+0.0279	-1.6679	-0.4448	+0.5165
K_9	-1.7703	+1.0275	-0.0409	+0.6819	+0.0521	+0.6061	-0.4093	-2.2382
K_{10}	-1.7263	+2.5915	+0.1979	+0.1240	-0.0027	+0.3527	-1.1080	-5.0222
K_{11}	-1.6888	+1.5962	-0.2815	+0.3812	+0.0444	+0.0616	-2.0532	-3.0808
K_{12}	+0.7699	+0.1931	+0.6702	-0.2095	-0.0105	+0.0004	-0.7588	+0.8607
K_{13}	+1.8973	-3.7958	-0.2495	-0.0231	+0.0096	-0.2515	+0.6299	+6.0085

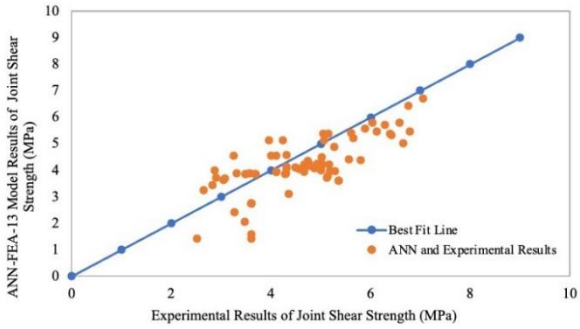

Figure 18. Comparison of the results between the ANN-FEA-13 model and ACI-318 in the prediction of shear strength of the unreinforced BCJ

Over the full testing dataset, the ACI-318 exhibited an average prediction-to-FEA ratio of 1.257, indicating a consistent overestimation of the joint shear strength. On the other hand, the ANN-FEA-13 model achieved an average prediction performance of 1.003, demonstrating excellent agreement with the FEA simulation. The results highlight the model's ability to reliably capture nonlinear relationships not explicitly represented in the standard code equations. Table 10 summarizes sample results comparing the ACI-318 and the ANN-FEA-13 predictions. The consistent bias in the ACI-318 predictions suggests that the ACI predicts higher shear strength and accordingly overestimates the joint capacity, whereas it underestimates the risk of failure of the BCJ joint. However, the ANN-FEA-13 predictions are more conservative, aligning with the requirements of resilience-based assessments of existing RC structures.

3.4 Comparison with Experimental Results from Literature

To evaluate the prediction accuracy of the ANN-FEA-13 model beyond the numerically generated samples, ANN-FEA-13 was compared with 80 exterior BCJ specimens reported in the literature. The specimens have variable geometries, material properties, reinforcement configurations, and axial load levels, and many fully/partially fall outside the ANN-FEA-13 model training and evaluation domain. Although several experimental specimens considered in this study were located outside the exact range of the ANN training dataset, the developed model demonstrated reasonable predictive performance.

This observation should not be interpreted as evidence of reliable extrapolation capability under all conditions. ANN models are fundamentally data-driven approaches, and their predictive accuracy generally decreases when applied to cases that differ significantly from the training distribution. What makes the performance high relative to the literature is that some input parameters are already within the training range, but their joint area was reinforced. The full details of the selected joint specimens are presented in Appendix C, and a summary of the supplementary material associated with this manuscript is shown in Table 11. Figure 19 shows the comparison between the ANN-FEA-13 model predictions of shear strength against the experimental results of 80 beam-column joint specimens reported in the literature.

Table 12 summarizes the results of the comparison for some selected specimens. Regardless of the inherent differences between the studied specimens and the BCJ sample configurations of the ANN-FEA-13, and noting that point-to-point comparison is not feasible due to differences between the FEA-based and experimentally observed failure mechanisms, the model achieved an overall prediction-to-experiment ratio of 0.915, indicating superior performance. 72 specimens out of 80, accounting for 90% of the overall experimental sample, were predicted within the 30% error range, and 51 specimens (63.8%) showed errors less than 20% in prediction using the ANN-FEA-13 model. The total average error for the 80 sample predictions of the ANN-FEA-13 model was 17.2%. Large error deviations were associated with specimens containing transverse reinforcement or having parameter combinations far from the training range, which is an expected model limitation. Although the ANN-FEA-13 model demonstrated satisfactory predictive performance based on the adopted accuracy indicators, it is important to note that the reported average prediction ratios and error values reflect overall model performance and do not fully capture the uncertainty associated with individual predictions. The reliability of ANN predictions is influenced by the size, quality, and distribution of the training dataset, and higher uncertainty may be expected for cases with limited representation within the input space. Nevertheless, the overall ANN-FEA-13 model performance indicates its ability to reliably extrapolate predictions to several unseen physical configurations, reinforcing its use as a primary screening tool for estimating the shear strength of joints and evaluating the resilience of old structures.

Table 10. Sample results of the comparison between the ANN-FEA-13 model and the ACI-318 code requirements for the prediction of shear strength of the unreinforced BCJ

No.	vjn FEA Result (MPa)	vjn ACI-318 (MPa)	vjn ANN-FEA-13 (MPa)	ACI/FEA result	ANN/FEA result
1	4.459	4.123	4.627	0.92	1.04
2	4.792	4.472	4.932	0.93	1.03
3	5.211	5.000	5.410	0.96	1.04
4	5.736	5.477	5.844	0.95	1.02
5	6.124	5.916	6.231	0.97	1.02
6	6.591	6.325	6.570	0.96	1.00
7	6.761	6.708	6.866	0.99	1.02
8	6.776	7.071	7.125	1.04	1.05
9	6.768	7.416	7.350	1.10	1.09
10	4.468	4.123	4.603	0.92	1.03
Average values for the full testing data set (6480 Samples)				1.257	1.003

Table 11. Statistical summary of model prediction errors for different loading types and reinforcement conditions

Loading Type	Reinforcement	Count	Mean Error %	Std. Dev. %
Cyclic	Reinforced	55	17.48%	12.66%
Cyclic	Unreinforced	10	19.99%	13.17%
Reversal Cyclic	Reinforced	8	10.34%	4.57%
Reversal Cyclic	Unreinforced	1	29.81%	0.00%
Aqua Static Cyclic	Reinforced	4	13.39%	10.26%
Monotonic	Unreinforced	2	17.32%	5.36%

Table 12. Sample of the comparison between the prediction of the ANN-FEA-13 model for shear strength against the experimental results of 80 beam-column joint specimens curated from literature

No.	Experimental Result (MPa)	ANN-FEA-13 (MPa)	ANN Prediction/ Experimental
1	4.310	4.568	1.060
2	5.800	4.385	0.756
3	4.100	4.555	1.111
4	5.560	4.408	0.793
5	5.280	3.969	0.752
6	5.044	5.369	1.065
7	5.001	3.997	0.799
8	5.613	5.409	0.964
9	4.662	3.931	0.843
10	5.153	5.391	1.046
Average ANN Prediction/Experimental (80 samples)			0.915

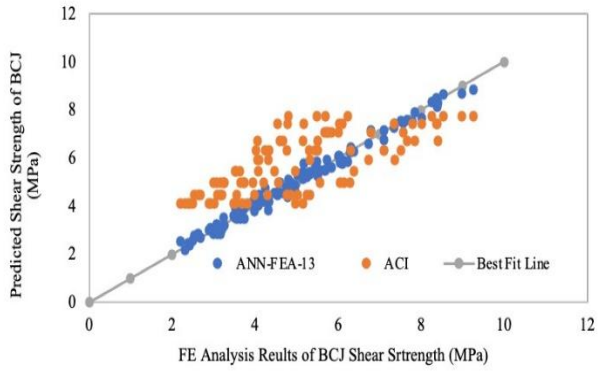

Figure 19. Comparison between the ANN-FEA-13 model predictions of shear strength and the experimental results of 80 beam-column joint specimens reported in the literature

4. Conclusion

The study developed a hybrid ANN-FEA model (ANN-FEA-13) for the prediction of shear strength of unreinforced exterior RC beam-column joints. The ANN-FEA-13 model was trained, validated and tested on a large and comprehensive dataset of 4320 joint shear failure simulations through a nonlinear finite element analysis in ABAQUS with concrete damage plasticity models, covering wide variations in geometry, reinforcement, material strength, and axial load. The ANN-FEA-13 model is formulated based on 7 selected input parameters (column and beam depth, concrete cylinder compressive strength, beam tension reinforcement yield strength and area, axial column load as a ratio of its capacity, and joint area). A feedforward artificial neural network model with 1 hidden layer and 13 neurons demonstrated the best performance, achieving an overall correlation of R = 0.962 and an RMSE of 0.367 MPa. The model's prediction accuracy was benchmarked against the ACI-318 provisions, using FEA results as the baseline for comparison. The model outperformed the ACI 318 predictions, which were found to overestimate the joint's shear capacity, suggesting an underestimation of the vulnerability of the joints in old buildings. Furthermore, the model demonstrated strong generalization when evaluated on 80 experimental specimens from the literature, achieving a 17.2% average error despite some differences in detailing and loading. Overall, the hybrid ANN-FEA-13 framework provides a fast, data-driven, and reliable tool for assessing the shear capacity of unreinforced exterior joints in RC buildings, offering improved accuracy compared to current design expressions. Future work should expand the model to include internal joints, cyclic degradation, joints with transverse reinforcement, and mixed failure mechanisms to further enhance its applicability.

Ethical issue

The authors are aware of and comply with best practices in publication ethics, specifically with regard to authorship (avoidance of guest authorship), dual submission, manipulation of figures, competing interests, and compliance with policies on research ethics. The authors adhere to publication requirements that the submitted work is original and has not been published elsewhere. All survey participants provided informed consent prior to participation, and the anonymity and confidentiality of all respondents were strictly maintained throughout the research process.

Data availability statement

The manuscript contains all the data. However, additional data will be provided by the corresponding author upon reasonable request.

Conflict of interest

The authors declare no potential conflict of interest.

References

[1] S. O. Shaaban IG, "Experimental behavior of full-scale exterior beam-column space joints retrofitted by ferrocement layers under cyclic loading," Case Studies in Construction, vol. 8, p. 61–78, 2018.

[2] J. H. Haido, "Prediction of the shear strength of RC beam-column joints using new ANN formulations," Structures, vol. 38, p. 1191–1209, 2022.

[3] S. M. Allam, H. M. Elbakry and I. S. Arab, "Exterior reinforced concrete beam column joint subjected to

monotonic loading," Alexandria Engineering Journal, vol. 57, p. 4133–4144, 2018.

[4] L. S. R. Salinas Guayacundo DR, "Nonlinear analysis of unreinforced beam-column joints," Inge CuC, vol. 16, p. 129–140, 2020.

[5] B. M. E.-K. N. Salado Castillo JG, "Seismic resilience of building inventory towards resilient cities," Resilient Cities and Structures, vol. 1, p. 1–12, 2022.

[6] B. M. S. A. S. K. Singh RR, "Resilience deficit index for quantification of resilience," Resilient Cities and Structures, vol. 1, pp. 1-9, 2022.

[7] Z. C. Christopoulos C, "Towards understanding, estimating and mitigating higher mode effects for more resilient tall buildings," Resilient Cities and Structures, vol. 1, p. 53–64, 2022.

[8] M. H. El-Naqeeb, B. S. Abdelwahed and S. E. El-Metwally, "Numerical investigation of RC exterior beam-column connection with different joint reinforcement detailing," Institution of Structural Engineers, vol. 38, p. 1570–1581, 2022.

[9] E. Ercan, B. Arisoy and a. O. B. Ertem, "Experimental Assessment of RC Beam-Column Connections with Internal and External Strengthening Techniques," Advances in Civil Engineering, vol. 2019, 2019.

[10] J. Melo, H. Varum and T. Rossetto, "Experimental assessment of the monotonic and cyclic behaviour of exterior RC beam-column joints built with plain bars and non-seismically designed," Engineering Structures, vol. 270, p. 114887, 2022.

[11] A. A. Maseer MS, "Enhancing performance of beam-column joints in reinforced concrete structures using carbon fiber-reinforced polymers (CFRP): A novel review," Hybrid Advances 10 , 2025.

[12] O. Algassem and R. L. Vollum, "Behaviour and design of monotonically loaded reinforced concrete external beam-column joints," Structures, vol. 52, p. 946–970, 2023.

[13] M. Risi, P. Ricci, G. Verderame and G. Manfredi, "Experimental assessment of unreinforced exterior beam-column joints," in 16th World Conference on Earthquake, 16WCEE 2017, Santiago Chile, 2017.

[14] C. R. Y. B. M. R. Mucedero G, "Estimation of seismic downtime for building retrofitting decision-making. Resilient Cities and Structures," vol. 4, p. 15–29, 2025.

[15] S. IH, "Machine Learning: Algorithms, Real-World Applications and Research Directions," SN Comput Sci 2, 2021.

[16] S. Golnaraghi, Z. Zangenehmadar, O. Moselhi and S. Alkass, "Application of Artificial Neural Network(s) in Predicting Formwork Labour Productivity," Advances in Civil Engineering, vol. 2019, 2019.

[17] S. Mangalathu, G. Heo and J.-S. Jeon, "Artificial neural network based multi-dimensional fragility development of skewed concrete bridge classes," Engineering Structures, vol. 162, pp. 166-176, 2018.

[18] S. Chatterjee, S. Sarkar, S. Hore, D. Nilanjan, A. Ashour, F. Shi and D. Le, "Structural failure classification for reinforced concrete buildings using trained neural network based multi objective genetic algorithm," Structural Engineering and Mechanics, vol. 63, no. 4, pp. 1598-6217, 2017.

[19] D.-C. Feng, Z.-T. Liu, X.-D. Wang, Z.-M. Jiang and S.-X. Liang, "Failure mode classification and bearing capacity prediction for reinforced concrete columns based on ensemble machine learning algorithm," Advanced Engineering Informatics, vol. 45, 2020.

[20] B. Todorov and A. MuntasirBillah, "Machine learning driven seismic performance limit state identification for performance-based seismic design of bridge piers," Engineering Structures, vol. 255, no. 0141-0296, 2022.

[21] H. Nguyen, T. Vu, T. P. Vo and H.-T. Thai, "Efficient machine learning models for prediction of concrete strengths," Construction and Building Materials, vol. 266, no. 0950-0618, 2020.

[22] J. Xu, W. Hong, J. Zhang, S. Hou and G. Wu, "Seismic performance assessment of corroded RC columns based on data-driven machine-learning approach," Engineering Structures, vol. 255, no. 0141-0296, 2022.

[23] L. Ali, F. Alnajjar, A. Jassmi, M. Gocho, W. Khan and A. Serhani, "Performance Evaluation of Deep CNN-Based Crack Detection and Localization Techniques for Concrete Structures," Sensors, vol. 21, no. 5, p. 1688, 2021.

[24] Z. L. A. R. H. R. Wang G, "Deformation and stress theory of surrounding rock of shallow circular tunnel based on complex variable function method," Applied Mathematics and Nonlinear Sciences, vol. 7, p. 629–640, 2022.

[25] A. M. Wakjira TG, "Hybrid machine learning-enabled multivariate bridge-specific seismic vulnerability and resilience assessment of UHPC bridges," Resilient Cities and Structures, vol. 4, p. 92–102, 2025.

[26] L. R. Hashemi A, "Seismic performance evaluation of mass timber buildings equipped with resilient and conventional friction devices," Resilient Cities and Structures, vol. 4, p. 103–115, 2025.

[27] A. A. H. Alwanas, A. A. Al-Musawi, S. Q. Salih, H. Tao, M. Ali and Z. M. Yaseen, "Load-carrying capacity and mode failure simulation of beam-column joint connection: Application of self-tuning machine learning model," Engineering Structures, vol. 194, p. 220–229, 2019.

[28] H. S. Marie, K. A. El-Hassan, E. M. Almetwally and M. A. El-Mandouh, "Joint shear strength prediction of beam-column connections using machine learning via experimental results," Case Studies in Construction Materials, vol. 17, p. e01463, 2022.

[29] S. Ramavath and S. R. Suryawanshi, "Optimal Prediction of Shear Properties in Beam-Column Joints Using Machine Learning Approach," International Journal of Engineering, vol. 37, no. 01, pp. 67-82, 2024.

[30] M. M. A. A. e. a. Jayasinghe SC, " A review on the applications of artificial neural network techniques for accelerating finite element analysis in the civil engineering domain," Comput Struct 310.

[31] B. R. Infante V, "Non-Proportional mixed mode plastic zones via finite elements and artificial neural networks," Theoretical and Applied Fracture Mechanics, p. 135.

[32] L. N. S. A. T. E. Chen PY, "A Method for automated development of model and fragility inventories of nonductile reinforced concrete buildings," Resilient Cities and Structures, vol. 2, pp. 87-103, 2023.
[33] ABAQUS, Abaqus Analysis User's Guide 6.13, Providence, RI: Dassault Systèmes Simulia Corp, 2013. https://wikifab.org/wiki/Abaqus_documentation_6.13_pdf
[34] K. Creel, "Transparency in Complex Computational Systems," Philosophy of Science, vol. 87, no. 4, pp. 568-589, 2020.
[35] M. Ajmal, D. Ahmed, M. H. Baluch, M. K. Rahman and T. Ayadat, "Consistent choice for cohesion and internal friction for concrete constitutive models," Innovative Infrastructure Solutions, vol. 8, no. 43, 2023.
[36] ACI 318-19 Committee, Building Code Requirements for Structural Concrete (ACI 318-19), Farmington Hills, Michigan : American Concrete Institute, 2019.
[37] J. B. Mander, M. J. N. Priestley and R. Park, "THEORETICAL STRESS-STRAIN MODEL FOR CONFINED CONCRETE," Journal of Structural Engineering, vol. 114, no. 8, pp. 1804-1826, 1988.
[38] S. J. Z. Y. Y. S. a. M. M. E. Ağcakoca, "Advanced Hybrid Modeling of Cementitious Composites Using Machine Learning and Finite Element Analysis Based on the CDP Model," Buildings, 2025.
[39] L. C. A. Y. T. J. a. J. S. K. Zheng, "Study on a Layered Finite Element Method for Hollow Concrete-Filled Steel Tube Columns," Advances in Civil Engineering, 2025.
[40] S. A. M. I. K. M. A. G. S. A. a. A. K. M. Ali, "Experimental Validation of Mander's Model for Low Strength Confined Concrete Under Axial Compression," in Second International Sustainability and Resilience Conference: Technology and Innovation in Building Designs(51154), 2020.
[41] B. Massicotte, A. E. Elwi and J. G. MacGregor, "Tension stiffening model for planar reinforced concrete members," ASCE Journal of Structural Engineering, vol. 116, no. 11, p. 3039–3058, 1990.
[42] M. Ajmal, Cyclic Response of Beam Column Joints Strengthened with Superelastic Shape Memory Alloys (SMAs) (PhD thesis), Dhahran: King Fahd University of Petroleum and Minerals, 2016.
[43] S. J. Hamil, Reinforced Concrete Beam-Column Connection Behaviour (PhD thesis), Durham, England: School of Engineering, University of Durham, 2000.
[44] The MathWorks Inc., MATLAB version: 9.7.0 (R2019b), Natick, Massachusetts: The MathWorks Inc., 2019.
[45] S. Alagundi and T. Palanisamy, "Neural network prediction of joint shear strength of exterior beam-column joint," Structures, vol. 37, p. 1002–1018, 2022.
[46] S. IH, "Machine Learning: Algorithms, Real-World Applications and Research Directions," SN Comput Sci 2 , 2021. https://doi.org/10.1007/s42979-021-00592-x
[47] K. A. M. Ali, C. Li, W. Han, S. Issa, M. H. Eid, S. F. Mahmoud and M. A.-E. Mohammed., "Performance evaluation and prediction of optimal operational conditions for a compact date seeds milling unit using feedforward neural networks," Scientific Reports, vol. 15, p. 4764 , 2025.
[48] M. Bauchy, Artificial Neural Networks and Deep Learning – Machine Learning for Engineers, California, Los Angeles: University of California, 2020. https://catalog.registrar.ucla.edu/course/2021/ecengrc147?siteYear=2021